Cathepsin B regulates hepatic lipid metabolism by cleaving liver fatty acid–binding protein

Received for publication, January 24, 2017, and in revised form, November 15, 2017 Published, Papers in Press, December 19, 2017, DOI 10.1074/jbc.M117.778365

Simeon Thibeaux, Shaila Siddiqi, Olga Zhelyabovska, Faisal Moinuddin, Michal M. Masternak, and Shadab A. Siddiqi[1]

From the Burnett School of Biomedical Sciences, College of Medicine, University of Central Florida, Orlando, Florida 32827

Edited by Thomas Söllner

Synthesis and secretion of hepatic triglycerides (TAG) associated with very-low-density lipoprotein (VLDL) play a major role in maintaining overall lipid homeostasis. This study aims to identify factors affecting synthesis and secretion of VLDL-TAG using the growth hormone–deficient Ames dwarf mouse model, which has reduced serum TAG. Proteomic analysis coupled with a bioinformatics-driven approach revealed that these mice express greater amounts of hepatic cathepsin B and lower amounts of liver fatty acid–binding protein (LFABP) than their wildtype littermates. siRNA-mediated knockdown of cathepsin B in McA-RH7777 cells resulted in a 39% increase in [^{3}H]TAG associated with VLDL secretion. Cathepsin B knockdown was accompanied by a 74% increase in cellular LFABP protein levels, but only when cells were exposed to 0.4 mM oleic acid (OA) complexed to BSA. The cathepsin B knockdown and 24-h treatment with OA resulted in increased CD36 expression alone and additively. Co-localization of LFABP and cathepsin B was observed in a distinct Golgi apparatus–like pattern, which required a 1-h OA treatment. Moreover, we observed co-localization of LFABP and apoB, independent of the OA treatment. Overexpression of cathepsin B resulted in decreased OA uptake and VLDL secretion. Co-expression of cathepsin B and cathepsin B–resistant mutant LFABP in McA-RH7777 cells resulted in an increased TAG secretion as compared with cells co-expressing cathepsin B and wildtype LFABP. Together, these data indicate that cathepsin B regulates VLDL secretion and free fatty acid uptake via cleavage of LFABP, which occurs in response to oleic acid exposure.

The liver is responsible for the synthesis and secretion of very-low-density lipoproteins (VLDL).[2] This important physiological process helps to distribute energy-rich triglycerides to peripheral tissues and to maintain triglyceride balance within the hepatocyte. The secretion process is tightly regulated, as the development of hepatic steatosis leads to defective secretion of VLDL (1). Steatosis is characterized by the formation of triglyceride-rich lipid droplets within the cell, which may progress into non-alcoholic fatty liver disease. When triglyceride availability is high VLDL, synthesis may continue unimpeded (2), and the blood becomes rich with remnant low-density lipoprotein particles, which can become oxidized and taken up by macrophages dwelling within major arteries (3). This drives the formation and propagation of atheromatous plaque, which is the major underlying cause of cardiovascular disease (4). This highlights the importance of understanding the mechanisms responsible for regulating the process of VLDL assembly and secretion.

Triglycerides are derived from the esterification of free fatty acids (FFA) to glycerol. FFA are delivered from the portal vein, chylomicron remnants, and lipolysis in adipose tissue and can be synthesized *de novo* in the liver (5). Import of FFA across the plasma membrane is mediated by CD36, also known as free fatty acid translocase (6). After membrane translocation, triglyceride synthesis occurs in the smooth endoplasmic reticulum membrane, where liver fatty acid–binding protein (LFABP) delivers the fatty acid substrate to avoid the detergent-like effects of non-esterified free fatty acids within the cell (7). Very-low-density lipoprotein production begins with the simultaneous synthesis and translocation of apolipoprotein B100 (apoB100) on the rough endoplasmic reticulum (ER). For the stability of this molecule to be maintained, initial lipidation by microsomal triglyceride transfer protein must occur in the rough ER (8). In the absence of sufficient triglyceride, the poorly lipidated apoB100 molecule is sorted for degradation, which is the fate of most apoB100 molecules (2). Thus, the availability of LFABP-delivered FFA for triglyceride synthesis in the ER represents the first line in regulating VLDL assembly.

Regulation of VLDL secretion, lipolysis, and gene expression by growth hormone has been long established *in vivo* (9). Exogenous administration of growth hormone, which has been used commercially as an anti-aging product, medically as a form of hormone replacement, and industrially for the growth of livestock, has been shown to increase VLDL secretion as well as triglyceride esterification by hepatocytes *in* vitro (10). Growth

This study was supported by NIDDK, National Institutes of Health (NIH), Grant R01 DK081413 (to S. A. S.) and NIA, NIH, Grant R01 AG032290 (to M. M. M.). The authors declare that they have no conflicts of interest with the contents of this article. The content is solely the responsibility of the authors and does not necessarily represent the official views of the National Institutes of Health.

[1] To whom correspondence should be addressed: Burnett School of Biomedical Sciences, College of Medicine, University of Central Florida, 6900 Lake Nona Blvd., Rm. 349, Orlando, FL 32827. Tel.: 407-266-7041; Fax: 407-266-7002; E-mail shadab.siddiqi@ucf.edu.

[2] The abbreviations used are: VLDL, very-low-density lipoprotein; IPG, immobilized pH gradient; 2D-DIGE, two-dimensional differential gel electrophoresis; FFA, free fatty acid(s); LFABP, liver fatty acid–binding protein; ER, endoplasmic reticulum; TNFα, tumor necrosis factor α; VTV, VLDL transport vesicle; PG-VTV, post-Golgi VTV; TAG, triglyceride(s); OA, oleic acid; dpm, disintegrations/min; NAFLD, non-alcoholic fatty liver disease; FBS, fetal bovine serum; ANOVA, analysis of variance.

hormone increases triglyceride availability for VLDL synthesis, as both VLDL secretion and cellular triglyceride content increase in parallel (11) due to increased availability of free fatty acids for triglyceride synthesis, which occurs independent of increased lipolysis in peripheral tissues. The exact molecular mechanism by which exogenous growth hormone regulates fatty acid availability for triglyceride synthesis has not been established and warrants further study due to the importance of this process in maintaining lipid homeostasis.

Interestingly, cathepsin B knockout mice are resistant to diet-induced hepatic steatosis (12). Despite being initially characterized as a lysosomal protease, cytosolic localization of cathepsin B in response to oleic acid and tumor necrosis factor α (TNFα) in a Bax-dependent manner has been observed (13). This suggests an intimate relationship between the cytosolic activity of cathepsin B and VLDL secretion, as both processes depend upon hepatic free fatty acid flux. Compounding the blatant nature of this association is the fact that cytosolic localization of cathepsin B correlates with disease severity in patients with non-alcoholic fatty liver disease (12). It has also been shown that in this population, decreased hepatic cathepsin B levels accompany increased serum triglycerides, suggesting a role for cathepsin B in worsening dyslipidemia. Cathepsin B has also been described previously as the β-secretase responsible for cleaving amyloid precursor protein in Alzheimer's disease, which provided insight into possible targets of cathepsin B degradation (12, 14) as specific cleavage of peptides on the C-terminal side of the cognate Val-Lys-Met sequence by cathepsin B was established *in vitro*. After cross-referencing this sequence with the VLDL transport vesicle (VTV) proteome, we identified LFABP as a candidate protein that may be regulated by cathepsin B cleavage (15).

In the present study, we sought to identify the mechanism by which growth hormone regulates triglyceride availability for VLDL synthesis *in vitro*. Ames dwarf mice lack an anterior pituitary gland and growth hormone secretion due to a naturally occurring mutation in the *prop-1* gene (16). This deficiency of growth hormone leads to reduced VLDL triglyceride secretion compared with wildtype littermates (17), which makes the model an exceptional candidate for identifying factors that relate growth hormone to VLDL secretion. To identify proteins that may be related to reduced VLDL secretion, we performed two-dimensional differential gel electrophoresis (2D-DIGE) analysis of hepatocyte whole-cell lysates isolated from Ames dwarf mice compared with their wildtype littermates. Our data indicate that Ames dwarf mouse liver expresses greater amounts of cathepsin B and less LFABP than wildtype littermates. With this information, we proceeded to examine the role of cathepsin B in VLDL secretion and regulation of FFA-trafficking protein expression in rat hepatoma cells (McA-RH7777 cells) *in vitro*. We report that cathepsin B regulates FFA availability for triglyceride synthesis by degradation of LFABP and regulation of CD36 expression, which occurs in conjunction with oleic acid exposure. This in turn regulates the rate of VLDL secretion in an oleic acid–dependent manner.

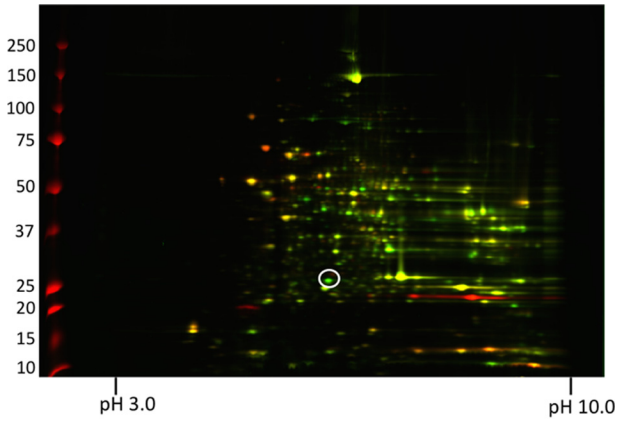

Figure 1. 2D-DIGE analysis of Ames dwarf whole-cell lysates. Shown is 2D-DIGE analysis of hepatic proteins from Ames dwarf (df/df) and WT mice. Whole-cell lysate proteins (300 μg) from hepatocytes of df/df and WT mice were labeled with Cy3 and Cy5 dye, respectively. Post-labeling, equal amounts of proteins from each sample were mixed together and solubilized in 2D gel buffer followed by isoelectric focusing using a total of 50,500 V-h. After equilibration, proteins were separated by 4–20% SDS-PAGE, and the gel was scanned utilizing Typhoon TRIO (GE Healthcare).

Results

Differential protein expression in Ames dwarf whole-cell lysates

In an attempt to identify factors that affect synthesis and secretion of VLDL-TAG, we decided to use the Ames dwarf mice because these growth hormone–deficient mice have reduced serum TAG along with increased hepatic TAG levels (18). We first sought to identify proteins that were differentially expressed in Ames dwarf mice livers that could explain their reduced VLDL secretion and serum TAG when compared with their wildtype littermates. Differential analysis of protein expression in Ames dwarf mice livers was performed by 2D-DIGE against matched samples from their wildtype littermates. Cy3 dye (*green*) was used to label Ames dwarf whole-cell lysates, and wildtype samples were labeled with Cy5 dye (*red*). Of several proteins that were uniquely or highly expressed in Ames dwarf mice, we identified a protein spot (*white circle*; Fig. 1) at ~25 kDa with an isoelectric point of 5.0–5.5, which was putatively identified as cathepsin B by cross-referencing with the ExPASy protein data bank. This protein was of particular interest because of its relevance to the current study. Our results indicate that Ames dwarf liver (Fig. 1) expresses greater amounts of cathepsin B than wildtype littermates.

We validated this observation with immunoblot analysis, which shows 227% increased expression of cathepsin B in (df/df) whole cell lysates when compared with wildtype littermates (Fig. 2, *A* and *B*). We decided to further investigate the potential role of cathepsin B in regulating VLDL assembly due to its robust expression in the liver of Ames dwarf mice and previous studies indicating that cathepsin B knockout mice are resistant to diet-induced hepatic steatosis (19). We hypothesized that the previously reported phenotype of reduced VLDL secretion may be in part due to increased expression of cathepsin B, leading to decreased expression of VLDL and FFA trafficking proteins as a result of cathepsin B cleavage. Interestingly, we observed a 56% decrease in expression of the FFA-trafficking

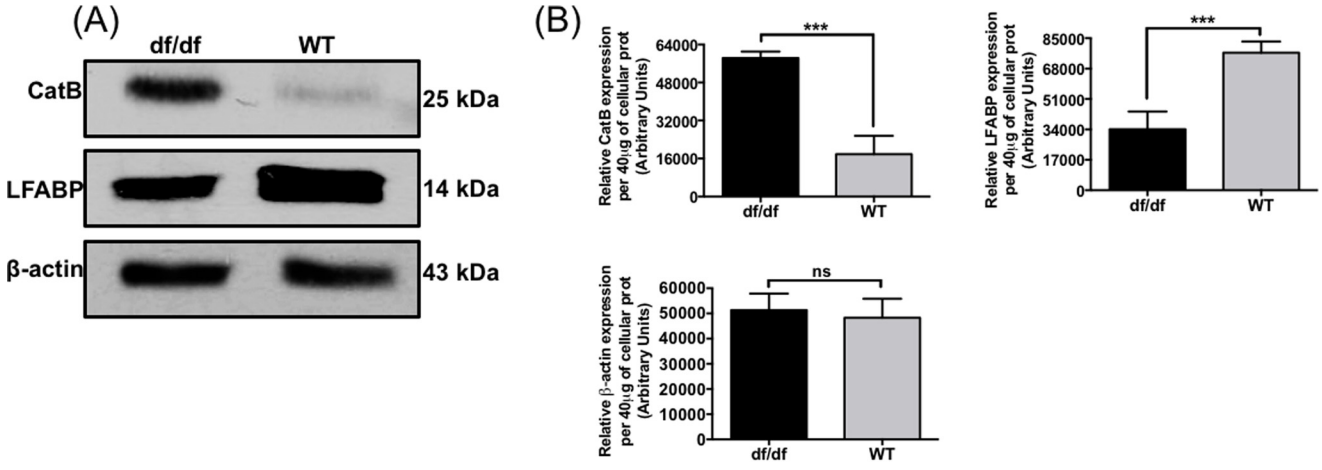

(C)

Wild-type LFABP

```
  1 MNFSGKYQVQ SQENFEPFMK AMGLPEDLIQ KGKDIKGVSE IVHEGKKVKL TITYGSKVIH
 61 NEFTLGEECE LETMTGEKVK AVVKMEGDNK MVTTFKGIKS VTEFNGDTIT NTMTLGDIVY
121 KRVSKRI
```

Figure 2. Cathepsin B and LFABP expression in Ames dwarf mice. *A*, immunoblots of hepatocyte whole-cell lysates of Ames dwarf (df/df) and WT mice. 40 μg of protein from whole-cell lysates was resolved on a 12% SDS-polyacrylamide gel, trans-blotted onto a nitrocellulose membrane, and probed with the indicated antibody. *B*, the amount of cathepsin B (*CatB*), LFABP, and β-actin per 40 μg of fraction protein (as shown in *A*) was determined by analyzing protein band density using ImageJ (National Institutes of Health). The results are the mean $\pm$ S.D. (*error bars*) ($n = 4$). *Bars labeled* with *asterisks* show *p* values using one-way ANOVA: ***, $p < 0.001$. *Bars labeled* with *ns* show non-significant *p* values. *C*, the sequences of established VTV protein components, which were previously identified by our laboratory (15), were mined from the UniProt protein database. The library of protein sequences was scanned for the VKM sequence recognized by cathepsin B using the Microsoft Word search function. LFABP was the only identified protein.

protein LFABP in (df/df) hepatocyte whole-cell lysates when compared with wildtype littermates (Fig. 2, *A* and *B*).

Previous studies have established that cathepsin B cleaves the proteins at the Val-Lys-Met (VKM) sequence *in vitro* (14). Our laboratory has previously published a comprehensive proteomic analysis of the VTV (15), which was used to compile a list of relevant proteins containing this sequence, which were all retrieved from the UniProt protein data bank. We were able to identify the VKM cleavage sequence within LFABP (Fig. 2*C*), a protein that has been implicated in trafficking fatty acids to the ER from the cell surface receptor CD36, also known as FFA translocase (20). It is well-established that apoB translation occurs at a somewhat steady rate and that apoB stability depends upon ER TAG availability (5). Thus, we proposed a mechanism in which cathepsin B restricts the flow of FFA to the ER for TAG synthesis by cleavage of LFABP. This would lead to reduced VLDL secretion by limiting ER TAG availability. This observation provides a potential mechanistic basis for the observed decrease in VLDL secretion seen in Ames dwarf mice as well as the increased rate of TAG esterification and VLDL secretion induced by GH administration. These observations may also provide insight into the role of the cathepsin B in the progress of NAFLD from simple steatosis by disrupting normal secretion of VLDL and uptake of FFA.

Impact of cathepsin B siRNA treatment on FFA-trafficking protein expression and VLDL secretion

To substantiate this hypothesis, we wanted to determine whether genetic knockdown of cathepsin B would lead to increased LFABP protein levels. Treatment with cathepsin B–specific siRNA delivered by Lipofectamine resulted in an 80% decrease in expression of the cathepsin B protein when compared with whole-cell lysates from control siRNA–treated cells (Fig. 3, *A* and *B*). Under the conditions of cathepsin B knockdown in McA-RH7777 cells, 1 h of 0.4 mM OA complexed with BSA treatment led to a 74% increase in levels of LFABP protein when compared with control siRNA–treated cells (Fig. 3, *A* and *B*). The observed difference in LFABP protein levels was not observed when cells were deprived of oleic acid stimulation (data not shown). This provides evidence for a mechanism in which cathepsin B cleavage of cytosolic LFABP occurs in an oleic acid– dependent manner.

A pulse-labeling approach was used to determine whether cathepsin B knockdown increases VLDL secretion. We tested this under the conditions of treatment with 0.4 mM OA complexed with BSA for 24 h as well as treatment with 0.2 mM BSA alone in PBS to analyze the impact of cathepsin B knockdown under conditions of elevated and reduced FFA availability, respectively. Interestingly, McA-RH7777 cells treated with 0.4 mM OA complexed with BSA for 24 h and cathepsin B–specific siRNA express a 70% greater amount of the cell surface FFA translocase CD36 when compared with OA-treated cells transfected with control siRNA (Fig. 3, *C* and *D*). Without pretreatment with 0.4 mM OA complexed with BSA, cathepsin B knockdown alone resulted in a 31.5% increase in CD36 expression relative to control siRNA (Fig. 3, *C* and *D*). Under conditions of OA pretreatment and cathepsin B knockdown, we observed a 39% increase in TAG secretion into the medium after 1 h when compared with control siRNA (Fig. 4*A*) as measured by

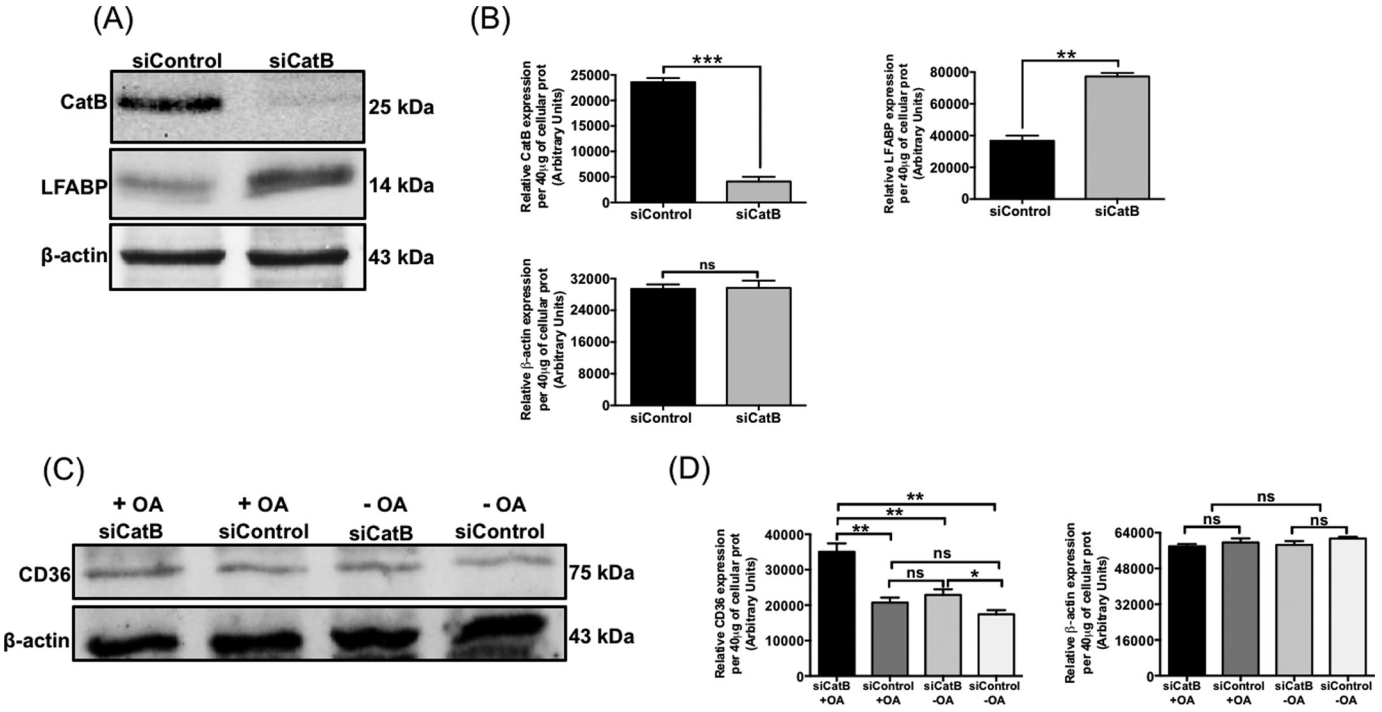

Figure 3. Knockdown of cathepsin B by siRNA transfection increases LFABP and CD36 expression in McA-RH7777 cells. *A*, McA-RH7777 cells were transfected with either control siRNA (*siControl*) or cathepsin B siRNA (*siCatB*), followed by 1-h treatment with 0.4 mM OA-BSA. 40 μg of protein from whole-cell lysates of either siControl or siCatB cells was resolved on a 12% SDS-polyacrylamide gel, trans-blotted onto a nitrocellulose membrane, and probed with the indicated antibody. *B*, the amount of cathepsin B (*CatB*), LFABP, and β-actin per 40 μg of cellular protein (as shown in Fig. 3*A*) was determined by analyzing protein band density using ImageJ. The results are the mean ± S.D. (*error bars*) ($n = 4$). *Bars labeled* with *asterisks* show *p* values using one-way ANOVA: **, $p < 0.005$; ***, $p < 0.001$. *Bars labeled* with *ns* show non-significant *p* values. *C*, samples analyzed were representative whole-cell lysates from a pulse-chase experiments with OA-BSA pretreatment. Cells were treated with OA-BSA (+*OA*) or just BSA (−*OA*), as indicated. ImageJ was used for quantification. *D*, the amount of CD36 and β-actin per 40 μg of fraction protein (as shown in Fig. 3*C*) was determined by analyzing protein band density using ImageJ. The results are the mean ± S.D. ($n = 3$). *Bars labeled* with *asterisks* show *p* values using one-way ANOVA: *, $p < 0.05$; **, $p < 0.005$. *Bars labeled* with *ns* show non-significant *p* values.

[^{3}H]TAG dpm counting. The observed increase in [^{3}H]TAG was maintained above 20% through the 2-, 4-, and 6-h time points (Fig. 4*A*). Without 24-h OA pretreatment, we observed a 15% increase in TAG secretion after 1 h relative to the control siRNA (Fig. 4*A*), which remained above 10% through the 2-, 4-, and 6-h time points but did not meet statistical significance.

We then sought to determine whether the increase in TAG secretion observed under conditions of cathepsin B knockdown was due to an increased number of VLDL particles secreted. The VLDL particle contains only one apoB molecule, whereas TAG content may vary slightly (21). As such, the number of VLDL particles secreted will be proportional to apoB secretion. Medium time points analyzed in the pulse-labeling experiment were subjected to immunoblotting, and the results show that cathepsin B knockdown resulted in a 115% increase in secretion of apoB into the medium relative to cells treated with control siRNA at the 1-h time point (Fig. 4*B*), which was consistent across the remaining time points. These results indicate that cathepsin B knockdown leads to an increased number of VLDL secreted from McA-RH7777 cells, which is in line with our proposed mechanism.

With this established, we sought to determine to what extent cathepsin B knockdown would impact cellular TAG content in McA-RH7777 cells after the 24-h chase period. An equal mass of whole-cell lysate (50 μg) from knockdown and control siRNA–treated samples was subjected to TAG extraction, and the final organic phase containing TAG was analyzed by [^{3}H]TAG dpm counting. Cathepsin B knockdown resulted in a 32% decrease in cellular [^{3}H]TAG content after a 1-h chase period (Fig. 4*C*). This result is expected and occurs as a result of increased VLDL-TAG secretion, which was observed under these conditions (Fig. 4, *A* and *B*). These data suggest that the observed increase in VLDL secretion is a result of increased LFABP and CD36 levels (Fig. 3, *A*–*D*), secondary to cathepsin B knockdown. This promotes greater FFA availability for TAG synthesis in the ER, which leads to increased stability of nascent VLDL, resulting in increased secretion of VLDL. This process occurred in an oleic acid– dependent manner, suggesting cleavage of LFABP that requires translocation of cathepsin B from the lysosome.

Overexpression of cathepsin B decreases VLDL secretion and cellular TAG

To increase our confidence in the proposed mechanism, we decided to overexpress cathepsin B in McA-RH7777 cells. We optimized an overexpression protocol using the pCI-Neo vector containing the cathepsin B gene insert. After transfection with the plasmid-containing insert, we observed a significant (240%) increase in cathepsin B expression relative to control cells transfected with the empty vector (Fig. 5, *A* and *B*). To determine the effects of cathepsin B overexpression on LFABP and CD36, we treated McA-RH7777 cells (cathepsin B–overexpressing and control) with 0.4 mM OA complexed with BSA for 1 h and carried out immunoblotting. Our immunoblot

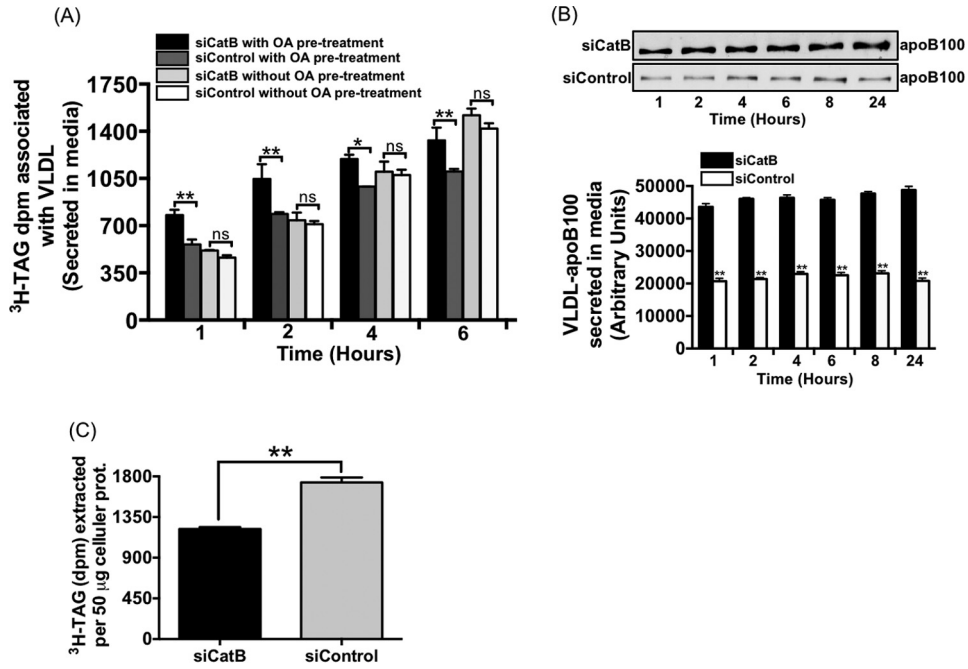

Figure 4. Cathepsin B knockdown increases VLDL secretion and reduces cellular TAG in McA-RH7777 cells. *A*, 0.3×10^6 McA-RH7777 cells were plated in each well of two 6-well plates and transfected using Lipofectamine RNAiMAX at a final concentration of 25 nM cathepsin B-specific siRNA (*siCatB*) or siRNA control (*siControl*). 24 h after transfection, three wells of each were supplemented with 0.4 mM OA complexed with BSA (with OA pretreatment) or 0.2 mM BSA alone (without OA pretreatment). 48 h after transfection, each well was washed and subjected to a 1-h pulse with OA-BSA– and BSA– bound 2-μCi [^{3}H]oleic acid in DMEM supplemented with 5% FBS. The pulse was removed, and each well was washed twice with fresh medium to remove residual label and filled to 3 ml with DMEM supplemented with 0.5% FBS. 200-μl aliquots of medium were collected at the indicated time points, TAG was extracted (see "Experimental procedures"), and [^{3}H]TAG dpm were determined. The data are the mean ± S.D. (*error bars*) ($n = 6$). *Bars labeled* with *asterisks* show *p* values using one-way ANOVA: *, $p < 0.01$; **, $p < 0.002$. *Bars labeled* with *ns* show non-significant *p* values. *B*, 30 μl of medium from cells treated with cathepsin B–specific siRNA (*siCatB*) or siRNA control (*siControl*) at the indicated pulse-chase time points was resolved on a 12% SDS-polyacrylamide gel, trans-blotted onto a nitrocellulose membrane, and probed with the indicated antibody. The amount of secreted VLDL-apoB100 was determined by analyzing protein band density using ImageJ. The results are the mean ± S.D. ($n = 3$). *Bars labeled* with *asterisks* show *p* values compared with control siRNA using one-way ANOVA: **, $p < 0.001$. *C*, 50 μg of protein from McA-RH7777 whole-cell lysates treated with cathepsin B–specific siRNA (*siCatB*) or siRNA control (*siControl*) was adjusted to a final volume of 200 μl with PBS. The diluted lysates were then subjected to solvent TAG extraction as described under "Experimental procedures," and [^{3}H]TAG dpm were determined. The data are the mean ± S.D. ($n = 3$). *Bars labeled* with *asterisks* show *p* values compared with control siRNA using one-way ANOVA: **, $p < 0.005$.

analysis of McA-RH7777 whole-cell lysates clearly indicated that cells that were overexpressing cathepsin B and treated with 0.4 mM OA complexed with BSA for 1 h expressed significantly less LFABP than control cells treated similarly and expressing only the empty vector (Fig. 5, *A* and *B*). The same conditions resulted in significantly decreased CD36 expression (Fig. 5, *A* and *B*). We speculated that cells overexpressing cathepsin B would secrete a reduced VLDL as a result of decreased FFA uptake and TAG synthesis. We performed a similar pulse-labeling protocol as was described for siRNA treatment, with the exception of withholding 24-h OA-BSA pretreatment. Secretion of TAG into the medium was decreased by 24% after 2 h in cells overexpressing cathepsin B, as measured by [^{3}H]TAG dpm counts, and remained above a 15% decrease through the 6- and 24-h time points (Fig. 5*C*). This result is in line with the proposed mechanism in which LFABP cleavage by cathepsin B results in reduced TAG availability for VLDL secretion.

With this in mind, we sought to determine the impact of cathepsin B overexpression on cellular retention of our [^{3}H]TAG. We found that overexpression of cathepsin B led to a 23% decrease in cellular [^{3}H]TAG compared with control cells expressing only the empty vector after the 24-h pulse chase (Fig. 5*D*). We surmised that this could be attributed to reduced uptake of the [^{3}H]oleic acid during the pulse phase. This suggests that the observed reduction on [^{3}H]TAG secretion seen under conditions of cathepsin B overexpression can be attributed to decreased FFA uptake as a result of cathepsin B regulation of LFABP and CD36 protein levels.

Thus far, we have established that knockdown of cathepsin B leads to increased LFABP and CD36 when cells are treated with physiologically relevant concentrations of 0.4 mM OA complexed with BSA. We have also established that this leads to increased VLDL secretion, as measured by [^{3}H]TAG dpm counts and VLDL-apoB100, and a decrease in cellular [^{3}H]TAG. Furthermore, cathepsin B overexpression leads to decreased FFA uptake and reduced VLDL secretion as a by-product of this mechanism. In our proposed mechanism, cytosolic cathepsin B regulates LFABP, which in turn regulates TAG availability for VLDL secretion.

OA treatment is required for co-localization of LFABP with cathepsin B but not with apoB

Our next goal was to visualize interaction of LFABP with apoB (a VLDL core protein) and cathepsin B. Dual labeling of McA-RH7777 cells was performed to test whether LFABP co-localizes with apoB as well as cathepsin B. Co-localization of LFABP with apoB and cathepsin B was performed with or without 0.4 mM OA complexed with BSA (OA-BSA) pretreatment to determine what impact these conditions have on interaction between the two proteins. In the absence of OA, when cells

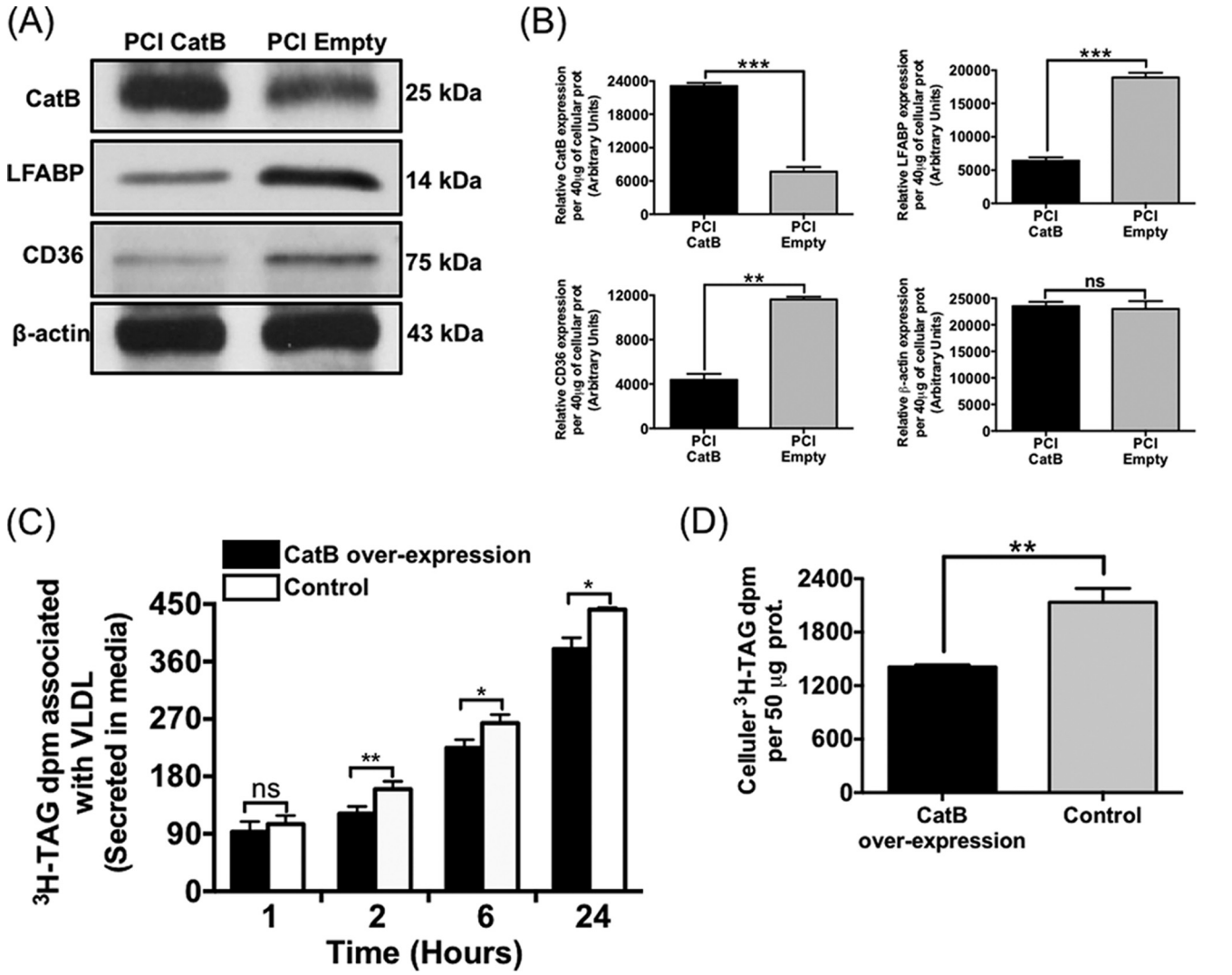

Figure 5. Cathepsin B overexpression decreases VLDL secretion and FFA uptake. *A*, McA-RH7777 cells (0.3×10^6) were plated in each well of two 6-well plates and transfected using Lipofectamine 2000 with each well containing a final mass of 2.5 μg of the PCI-Neo vector containing the cathepsin B gene insert (*PCI CatB*; $n = 3$) or empty vector (*PCI Empty*; $n = 3$). 48 h after transfection, each well was washed and subjected to a 1-h pulse, with 0.4 mM OA complexed with BSA and BSA-bound 2 μCi of [^{3}H]OA in DMEM supplemented with 5% FBS. The pulse was removed, and each well was washed twice with fresh medium to remove residual label and filled to 3 ml with DMEM supplemented with 0.5% FBS. McA-RH7777 cell lysate (40 μg of protein) was resolved on a 12% SDS-polyacrylamide gel, trans-blotted onto a nitrocellulose membrane, and probed with the indicated antibody. *B*, the amount of cathepsin B (*CatB*), LFABP, CD36, and β-actin per 40 μg of whole-cell lysate protein (as shown in Fig. 5*A*) was determined by analyzing protein band density using ImageJ. The results are the mean ± S.D. (*error bars*) ($n = 4$). *Bars labeled* with *asterisks* show p values using one-way ANOVA: **, $p < 0.002$; ***, $p < 0.001$. *Bars labeled* with *ns* show non-significant p values. *C*, McA-RH7777 cells (0.3×10^6) were plated in each well of two 6-well plates and transfected with PCI-Neo vector containing the cathepsin B gene insert ($n = 3$) or empty vector ($n = 3$) using Lipofectamine 2000 and subjected to the same pulse-chase protocol as described above (Fig. 5*A*). 200-μl aliquots of medium were collected at the indicated time points and subjected to TAG extraction as described under "Experimental procedures," and [^{3}H]TAG dpm were determined. The data are the mean ± S.D. ($n = 3$). *Bars labeled* with *asterisks* show p values using one-way ANOVA: *, $p < 0.02$; **, $p < 0.005$. *Bars labeled* with *ns* show non-significant p values. *D*, 50 μg of protein from McA-RH7777 whole-cell lysates treated with PCI-Neo vector containing the cathepsin B gene insert (*CatB overexpression*; $n = 3$) and empty vector (*Control*; $n = 3$) was adjusted to a final volume of 200 μl with PBS. The diluted lysates were then subjected to TAG extraction (see "Experimental procedures"), and the final organic layer containing [^{3}H]TAG was subjected to liquid scintillation counting to determine cellular retention of the [^{3}H]OA label incorporated into [^{3}H]TAG. The data are the mean ± S.D. ($n = 3$). *Bars labeled* with *asterisks* show p values using one-way ANOVA: **, $p < 0.002$.

were treated with 0.4 mM BSA alone (*BSA*), co-localization of LFABP with apoB was determined based on the presence of a *yellow* (Fig. 6*A*, *top right*) staining pattern in the merged LFABP/apoB image. However, we did not observe any difference in co-localization of LFABP and apoB when cells were treated with OA-BSA for 1 h (Fig. 6*A*, *bottom right*). To ascertain co-localization of LFABP with apoB, we quantified our data. As shown in Fig. 6*F*, a Pearson correlation coefficient of 0.92 was observed between LFABP and apoB after BSA treatment (no OA-BSA treatment), whereas 1 h after OA-BSA treatment, a Pearson correlation coefficient of 0.94 was observed. These data suggest that LFABP co-localizes with apoB independent of OA treatment.

Interestingly, no co-localization of LFABP and cathepsin B was observed when cells were treated with BSA alone (Fig. 6*B*, *top right corner*), indicating that under these conditions, the two proteins are segregated from each other in McA-RH7777 cells. However, when cells were subjected to 1 h of OA-BSA treatment, two very important changes in protein distribution occur. The staining pattern of LFABP formed a distinctive ring

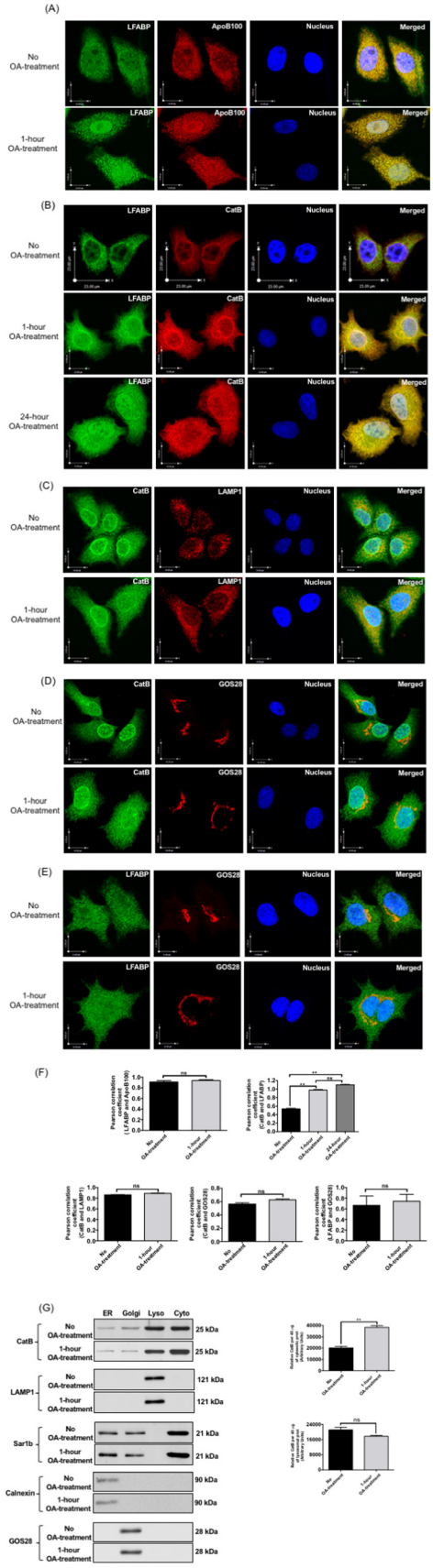

Figure 6. Effects of OA treatment on co-localization of cathepsin B with LFABP. *A*, McA-RH7777 cells were treated with either BSA alone (*No OA-treatment*; *top*) or 0.4 mM OA complexed with BSA (*1-hour OA-treatment*; *bottom*) for 1 h followed by double labeling with LFABP (FITC, *green*) and apoB (Texas red); the *merged image* shows co-localization. *B*, McA-RH7777 cells were treated with either BSA alone (*No OA-treatment*; *top*) or 0.4 mM OA complexed with BSA (1-h OA treatment; *middle*) for 1 h or 0.4 mM OA complexed with BSA for 24 h (24-h OA treatment; *bottom*) followed by double labeling with LFABP (FITC, *green*) and cathepsin B (*CatB*) (Texas red); the *merged image* shows no co-localization of proteins. *C*, McA-RH7777 cells were treated with either BSA alone (*No OA-treatment*; *top*) or 0.4 mM OA complexed with BSA (*1-hour OA-treatment*; *bottom*) for 1 h followed by double labeling with cathepsin B (*CatB*) (FITC, *green*) and LAMP1 (Texas red); the *merged image* shows co-localization. *D*, McA-RH7777 cells were treated with either BSA alone (*No OA-treatment*; *top*) or 0.4 mM OA complexed with BSA (*1-hour OA-treatment*; *bottom*) for 1 h followed by double labeling with cathepsin B (FITC, *green*) and GOS28 (Texas red); the *merged image* shows co-localization. *E*, McA-RH7777 cells were treated with either BSA alone (*No OA-treatment*; *top*) or 0.4 mM OA complexed with BSA (*1-hour OA-treatment*; *bottom*) for 1 h followed by double labeling with LFABP (FITC, *green*) and GOS28 (Texas red); the *merged image* shows co-localization. *A–E*, nuclei were stained with DAPI. *F*, co-localization of proteins was assessed by determining the Pearson correlation coefficient for all images (*A–E*). *G*, McA-RH7777 cells were treated with either BSA alone (*No OA-treatment*) or 0.4 mM OA complexed with BSA (*1-hour OA-treatment*) for 1 h, and ER, Golgi, lysosomes, and cytosol were prepared from the treated cells (see "Experimental procedures"). Equal amounts of proteins (40 μg) from the purified fractions of ER, Golgi, lysosomes (*Lyso*), and cytosol (*Cyto*) were resolved by 12% SDS-PAGE, transblotted onto a nitrocellulose membrane, and probed with specific antibodies against the indicated proteins. The data are representative of three independent experiments. The levels of CatB per 40 μg of either cytosolic or lysosomal protein (as indicated) under different treatments (either BSA alone (*No OA-treatment*) or 0.4 mM OA complexed with BSA (*1-hour OA-treatment*)) were determined by analyzing protein band density using ImageJ. The results are the mean ± S.D. (*error bars*) ($n = 3$). *Bars labeled* with *asterisks* show *p* values using one-way ANOVA: **, $p < 0.001$.

with a Golgi-like pattern, which is not evident with BSA-alone treatment (Fig. 6*B*, *top left* and *middle left*), and cathepsin B staining became diffuse and consistent with a cytosolic distribution (Fig. 6*B*, *second column* from the *left*, *bottom two panels*). Co-localization of LFABP and cathepsin B was observed in a diffuse cytosolic pattern as well as a more concise and distinctive pattern, which is consistent with localization to the Golgi apparatus (Fig. 6*B*, *far right middle panel*). In both dual-labeling experiments, OA-BSA treatment resulted in nuclear redistribution of LFABP, which is consistent with the previously described role of LFABP in delivery of hydrophobic ligands to the nucleus (Fig. 6, *A* and *B*). After a 24-h treatment with OA-BSA, the diffuse staining of cathepsin B is more apparent (Fig. 6*B*, *bottom left panels*), and the distinct ring of co-localization observed after 1 h is overwhelmed. We next quantified co-localization of LFABP and cathepsin B. 1 h after treatment with OA-BSA, cathepsin B and LFABP demonstrated a Pearson correlation coefficient of 0.99 (Fig. 6*F*, *top right*). Under the condition of BSA-alone treatment (control), a Pearson correlation coefficient of 0.5 was observed (Fig. 6*F*, *top right*). This indicates that cathepsin B and LFABP do not co-localize in the absence of OA but that 1 h after exposure to OA-BSA, there is a strong degree of co-localization between cathepsin B and LFABP. 24 h after treatment with OA-BSA, a Pearson correlation coefficient of 1.10 was observed, but the increase in co-localization due to prolonged OA-BSA exposure was not statistically significant (Fig. 6*E*, *top right*). This suggests that prolonged exposure to OA-BSA may slightly exacerbate the degree of cathepsin B redistribution, but 1 h of exposure is sufficient for significant interaction between the two proteins in the hepatic cytosol.

To validate the redistribution of cathepsin B from the lysosome, dual labeling with the lysosomal marker LAMP1

was performed after 1-h treatment of McA-RH7777 cells with either OA-BSA or BSA alone (Fig. 6*C*). As can be seen in Fig. 6*C*, OA-BSA treatment resulted in cytosolic distribution of cathepsin B (Fig. 6*C*, *bottom left*); however, there was no effect of OA treatment on LAMP1 distribution. Analysis of a Pearson correlation coefficient suggests that co-localization of cathepsin B and LAMP1 was unaffected by OA (Fig. 6*F*).

Dual labeling of cathepsin B (Fig. 6*D*) and LFABP (Fig. 6*E*) with the Golgi marker, GOS28, was performed to determine whether the punctate area of co-localization observed between LFABP and cathepsin B after 1 h of OA-BSA treatment was in fact at the Golgi level. A Pearson correlation coefficient of 0.55 was observed between cathepsin B and GOS28 without OA treatment (BSA alone–treated cells), whereas 1 h after OA-BSA treatment, a Pearson correlation coefficient of 0.6 was observed; this difference was not statistically significant (Fig. 6*F*). Similarly, analysis of a Pearson correlation coefficient suggests that co-localization of LAFABP and GOS28 was unaffected by OA (Fig. 6*F*); however, quantification by these means may be confounded by the nearly ubiquitous distribution of LFABP and the punctate distribution of GOS28. This suggests that a degree of co-localization between these two proteins does exist but that it is not impacted by OA (Fig. 6*F*). Interestingly, these data reflect close proximity of secreted cathepsin B and GOS28 in the Golgi compartment and suggest that lysosomal cathepsin B redistributed after OA-BSA treatment is not significantly recruited to the Golgi.

Because our data suggest that 1 h of exposure to OA-BSA significantly enhances the cytosolic localization of cathepsin B and in an attempt to directly demonstrate the localization of cathepsin B and LFABP under different conditions (with or without OA-BSA treatment), we isolated and purified ER, Golgi, lysosomes, and cytosols from McA-RH7777 cells that were treated with either BSA alone or 0.4 mM OA complexed with BSA for 1 h. The purity and characterization of these subcellular fractions were determined by marker proteins. LAMP1, a lysosomal marker protein, was present only in lysosomes, whereas ER, Golgi, and cytosol did not contain this protein (Fig. 6*G*). Sar1b, a cytosolic protein, was enriched in cytosol. ER and Golgi contain some Sar1b, which is consistent with prior published data (42); however, lysosomal fraction was devoid of Sar1b (Fig. 6*G*). Calnexin, an ER marker protein, was enriched in the ER, but other fractions were free from ER marker protein (Fig. 6*G*). GOS28 was present in Golgi, but the ER, lysosomes, and cytosol were free from Golgi marker protein (Fig. 6*G*). These data characterize subcellular fractions and demonstrate their purity. As shown in Fig. 6*G*, cathepsin B is predominantly present in lysosomes and cytosol, whereas ER and Golgi fractions contain significantly lesser amounts of cathepsin B. Interestingly, OA-BSA exposure resulted in a marked increase in cytosolic cathepsin B as compared with no OA treatment (BSA alone; Fig. 6*G*). We determined the levels of other proteins under both (with and without OA-BSA treatment) conditions; however, no significant difference was observed (Fig. 6*G*; protein band density data not shown).

Direct cleavage of LFABP by cathepsin B requires the VKM cognate sequence

To clearly demonstrate the specific role of cathepsin B in cleaving cytosolic LFABP, an overexpression protocol was established using wildtype LFABP and an LFABP mutant, which contained two amino acid point mutations in the cognate cleavage sequence (VKM → VNL) (Fig. 7*A*). To establish the validity of our overexpression protocol and the stability of our LFABP mutant, immunoblot analysis was performed using whole-cell lysates transfected with the PCIneo vector containing no insert, the LFABP mutant, and wildtype LFABP. Transfection with either the mutant or wildtype LFABP–containing vector resulted in a 100% increase in intensity of the 14 kDa LFABP band when compared with cells expressing the empty vector (Fig. 7*B*). There was no observable difference in intensity of the 14 kDa LFABP band between cells transfected with the mutant-containing plasmid and cells transfected with the wildtype LFABP–containing plasmid (Fig. 7*B*). This suggests equal efficiency in overexpression of the two proteins and no loss of stability due to the two amino acid point mutations.

Previous reports have shown that the three-amino acid sequence VKM is specifically recognized by cathepsin B *in vitro*, whereas the VNL sequence is not (14). Under conditions of co-transfection with the PCIneo plasmid containing the rat cathepsin B gene and the PCIneo plasmid containing the wildtype rat LFABP gene, there is a 40% decrease in intensity of the 14 kDa band representative of LFABP when compared with cells co-transfected with the cathepsin B plasmid and the VNL mutant LFABP plasmid (Fig. 7*C*). This demonstrates that disruption of the cognate VKM sequence in LFABP produces an LFABP mutant with resistance to cathepsin B cleavage. Importantly, this difference was dependent on treatment with 0.4 mM OA complexed with BSA (OA-BSA). When OA-BSA treatment was withheld in cells expressing only the empty pCI vector, the quantity of the 14-kDa LFABP protein contained in whole-cell lysates was increased 100% when compared with cells co-transfected with cathepsin B– and wildtype LFABP–containing plasmids, which were treated with OA-BSA (Fig. 7*C*). Co-transfection with the LFABP mutant and cathepsin B further demonstrated resistance of the mutant to OA-BSA–induced cleavage by cathepsin B, as a modest 30% decrease in intensity of the 14 kDa LFABP band was observed as a result of OA-BSA treatment (Fig. 7*C*). This supports our mechanism in which lysosomal cathepsin B redistributes to the hepatic cytosol after OA-BSA exposure, followed by cleavage of LFABP through recognition of the cognate VKM cleavage sequence. This observation supports the proposed role of cathepsin B in turnover of LFABP protein in the hepatic cytosol under normal conditions.

Lending further support to this mechanism is the production of a 10-kDa LFABP fragment induced by OA-BSA treatment, which is representative of the 82 N-terminal amino acids of LFABP, before the VKM cleavage sequence. This fragment was only observed under conditions of OA-BSA treatment and overexpression of LFABP or the cleavage resistant mutant, suggesting that cytosolic translocation of cathepsin B is necessary for the cleavage event described in this manuscript to occur. Mutation of the VKM cleavage sequence within LFABP

(A) **Cathepsin B-resistant LFABP (mutant LFABP)**

```
  1 MNFSGKYQVQ SQENFEPFMK AMGLPEDLIQ KGKDIKGVSE IVHEGKKVKL TITYGSKVIH
 61 NEFTLGEECE LETMTGEKVK AVVNLEGDNK MVTTFKGIKS VTEFNGDTIT NTMTLGDIVY
121 KRVSKRI
```

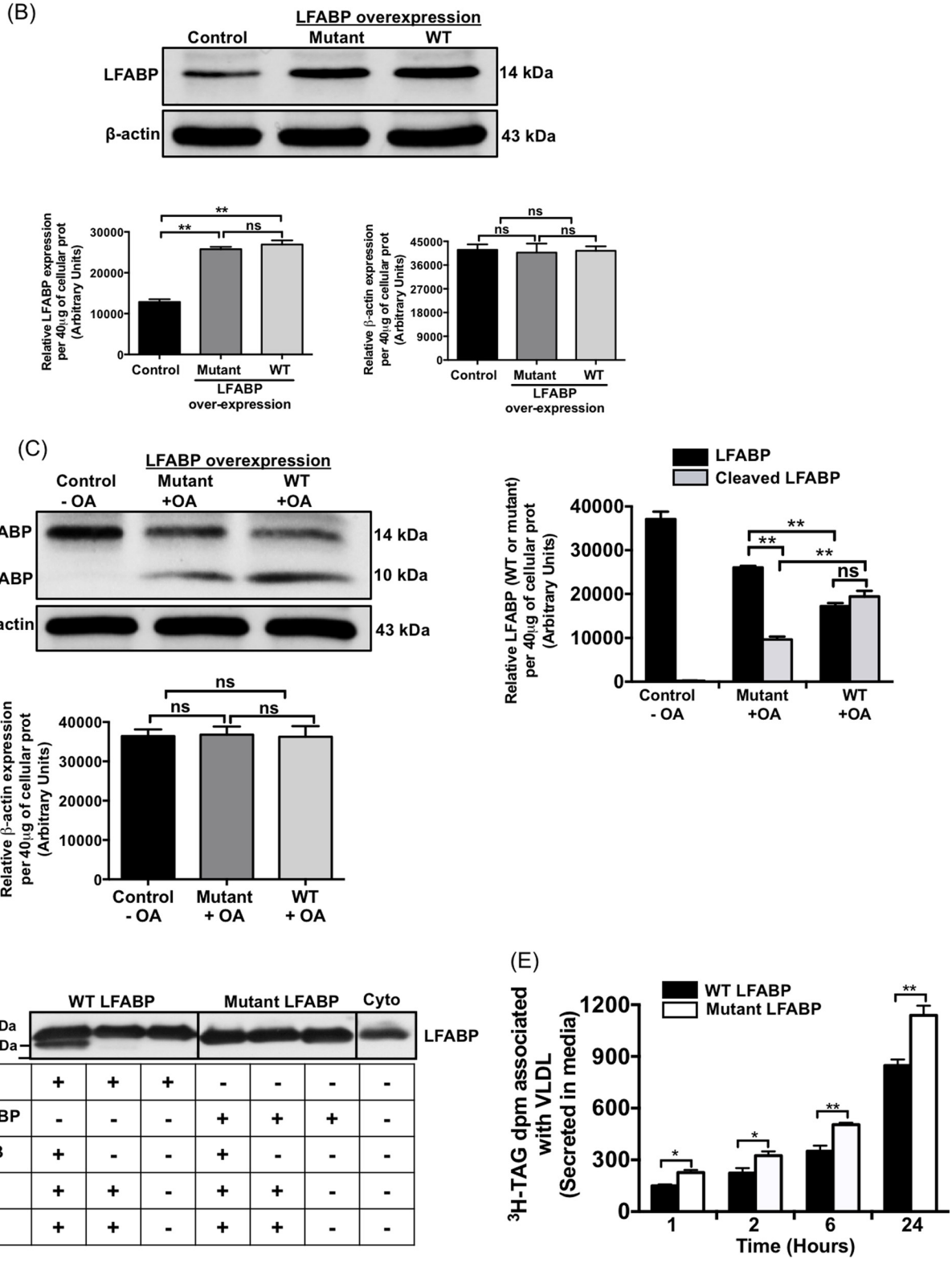

WT LFABP	+	+	+	-	-	-	-
Mutant LFABP	-	-	-	+	+	+	-
Cathepsin B	+	-	-	+	-	-	-
ATP	+	+	-	+	+	-	-
37 °C	+	+	-	+	+	-	-

resulted in a 50% reduction in intensity of the 10-kDa fragment (Fig. 7*C*). This lends further support for direct cleavage of LFABP at the VKM amino acid sequence by cathepsin B in hepatic cytosol.

To clearly demonstrate the direct cleavage of LFABP at the VKM amino acid sequence by cathepsin B, we treated either recombinant wildtype LFABP or mutant LFABP (VKM → VNL) with recombinant cathepsin B in the presence of ATP at 37 °C for 30 min. As was expected, our immunoblotting data suggest that wildtype LFABP and mutant LFABP migrated slightly differently on SDS-PAGE because of their different sequence. However, both proteins migrated very close to cytosolic LFABP (Fig. 7*D*). As shown in Fig. 7*D*, wildtype LFABP was cleaved when treated with cathepsin B in the presence of ATP, whereas mutant LFABP was unaffected under the same treatment. These data unambiguously prove our findings that cathepsin B directly cleaves LFABP at the VKM sequence.

With the biochemical mechanism of direct LFABP cleavage by cathepsin B established, we sought to validate the physiological relevance of our findings using the [^{3}H]TAG pulse-chase assay employed previously. Overexpression of the cleavage-resistant LFABP mutant resulted in a consistent and significant increase in [^{3}H]TAG secretion relative to cells overexpressing wildtype LFABP at 1, 2, and 6 h after the pulse was removed (Fig. 7*E*). The cleavage-resistant mutant displayed >20% increase in [^{3}H]TAG secretion into the medium when compared with cells overexpressing the wildtype LFABP after 24 h (Fig. 7*E*).

Discussion

The liver is responsible for maintaining energy homeostasis in the body through processes such as gluconeogenesis, fatty acid synthesis, and VLDL secretion. The precise balancing of these processes is required to maintain the necessary availability of each metabolite, and a failure to effectively regulate any poses serious consequences to general health. Hypersecretion of VLDL, which may occur as a result of insulin resistance, is a major risk factor for the development of atherosclerosis, highlighting the importance of developing a detailed understanding of this process (22, 23). Regulation of VLDL secretion is controlled by TAG availability as well as hormonal milieu, and degradation of apoB at the ER level has long been established as essential to directing this process (24). Flux of FFA to the ER is mediated by the lipid-binding and trafficking protein LFABP and the cell surface receptor CD36, which mediates the translocation of FFA across the cell membrane (7). TAG synthesized from this pool is added to the apoB molecule by microsomal triglyceride transfer protein as it is synthesized and simultaneously transported across the ER membrane, into the ER lumen. In the absence of sufficient TAG, this process is stalled. This causes hsp70 and hsp90 to bind to unfolded portions of the stalled apoB molecule, which is ubiquitinated by the E3 ligase gp78. This targets the core VLDL protein for degradation by the ERAD system in the cytosol (24). This highlights the importance of understanding processes that regulate FFA flux, which is essential to VLDL secretion and thus relevant to cardiovascular disease.

Once synthesized, the nascent VLDL particle must be trafficked between the ER and Golgi, and due to the size of nascent VLDL, a special packaging system is required for transportation (5, 25, 26). The VLDL transport vesicle, or VTV, is biochemically distinct from other COPII-derived vesicles that are responsible for the movement of nascent proteins between the ER and Golgi (15, 27, 28). Electron microscopy has revealed that VTVs, which contain apoB100, are 100–120 nm in diameter, whereas protein transport vesicles, which contain the secretory protein albumin, are 55–70 nm (25). This process is the rate-limiting step in the secretion of VLDL, which highlights the importance of understanding its regulation at the molecular level (25).

After delivery to the *cis*-Golgi lumen, several steps are required in maturation of the VLDL particle before secretion into the blood. The addition of complex carbohydrate moieties leads to increased buoyancy of the lipid-rich VLDL particle (29), whereas phosphorylation of the apoB backbone leads to

Figure 7. Effects of co-expression of cathepsin B and either wildtype LFABP or cathepsin B–resistant LFABP (mutant LFABP) on VLDL-TAG secretion. *A*, sequence of cathepsin B–resistant LFABP (mutant LFABP), which contains two amino acid point mutations in the cognate cleavage sequence (VKM → VNL). *B*, 0.3 × 10^6 McA-RH7777 cells were plated in each well of two 6-well plates and transfected using Lipofectamine 2000 with each well containing a final mass of 2.5 μg of the PCI-Neo vector containing the empty vector (*Control*; $n = 3$), mutant LFABP gene insert (*Mutant*; $n = 3$), or wildtype LFABP gene insert (*WT*; $n = 3$). 40 μg of protein from whole-cell lysates was resolved on a 12% SDS-polyacrylamide gel, trans-blotted onto a nitrocellulose membrane, and probed with the indicated antibody. The expression levels of wildtype LFABP (*WT*) and mutant LFABP (*Mutant*) and endogenous LFABP present in cytosol (*Control*) were determined by analyzing protein band density using ImageJ. The results are the mean ± S.D. (*error bars*) ($n = 3$). *Bars labeled* with *asterisks* show *p* values compared with control siRNA using one-way ANOVA: **, $p < 0.002$. *C*, 0.3 × 10^6 McA-RH7777 cells were plated in each well of two 6-well plates and co-transfected using Lipofectamine 2000 with each well containing a final mass of 2.5 μg of the PCI-Neo vector containing the empty vector (*Control*; $n = 3$), cathepsin B + mutant LFABP gene inserts (*Mutant*; $n = 3$), or cathepsin B + wildtype LFABP gene inserts (*WT*; $n = 3$). Post-transfection, cells were treated with BSA alone (−*OA*) or with 0.4 mM OA complexed with BSA (+*OA*) for 1 h. 40 μg of protein from whole cell lysates was resolved on a 12% SDS-polyacrylamide gel, trans-blotted onto a nitrocellulose membrane, and probed with the indicated antibody. The levels of wildtype LFABP (14 kDa; LFABP) and degraded LFABP (10 kDa; cleaved LFABP) under different treatments (−OA or +OA) were determined by analyzing protein band density using ImageJ. The results are the mean ± S.D. ($n = 3$). *Bars labeled* with *asterisks* show *p* values compared with control siRNA using one-way ANOVA: **, $p < 0.001$. *D*, either 1 μg of recombinant wildtype LFABP protein (WT LFABP) or 1 μg of recombinant mutant LFABP protein was incubated with or without 1 μg of recombinant cathepsin B at 37 °C for 30 min in the presence or absence of ATP, as indicated (total reaction volume 20 μl). Postincubation, the reaction was stopped by placing the tubes on ice and by adding 2× Laemmli's sample buffer, and the proteins were resolved by 12% SDS-PAGE, transblotted, and probed with specific antibodies against the LFABP protein. As a control, 40 μg of cytosolic proteins were probed by immunoblotting with anti-LFABP antibodies. The data are representative of three independent experiments. *E*, 0.3 × 10^6 McA-RH7777 cells were plated in each well of two 6-well plates and co-transfected using Lipofectamine 2000 with each well containing a final mass of 2.5 μg of the PCI-Neo vector containing the empty vector (*Control*; $n = 3$), cathepsin B + mutant LFABP gene inserts (*Mutant*; $n = 3$), or cathepsin B + wildtype LFABP gene inserts (*WT*; $n = 3$). 48 h after transfection, each well was washed and subjected to a 1-h pulse, with 0.4 mM OA complexed with BSA (+*OA*) and BSA-bound 2 μCi of [^{3}H]OA in DMEM supplemented with 5% FBS. The pulse was removed, and each well was washed twice with fresh medium to remove residual label and filled to 3 ml with DMEM supplemented with 0.5% FBS. 200-μl aliquots of medium were collected at the indicated time points and subjected to TAG extraction as described under "Experimental procedures," and [^{3}H]TAG dpm were determined. The data are the mean ± S.D. ($n = 3$). *Bars labeled* with *asterisks* show *p* values using one-way ANOVA: *, $p < 0.05$; **, $p < 0.002$.

structural rearrangements (30). The addition of further triglyceride within this compartment is still a matter of debate, with groups showing conflicting evidence for each case (31, 32). It has also been established that VLDL acquires apoA1 in the Golgi lumen, which is not present on the nascent VLDL during transport in the VTV, although the explicit role for this modification has not been established (33). Secretion of mature VLDL occurs by the formation of distinct post-Golgi VLDL transport vesicles (PG-VTVs), which are able to fuse with the plasma membrane (33). PG-VTVs are 300–350 nm in diameter and able to accommodate up to three mature VLDL particles (33).

The present study establishes that Ames dwarf mouse liver has 227% increased expression of the cysteine protease cathepsin B and 56% decreased expression of the FFA trafficking protein LFABP, which contributes to their observed reduction in VLDL secretion and serum TAG relative to wildtype littermates (17). We have also shown that LFABP co-localizes with apoB, suggesting that LFABP plays some not yet described role in the assembly and trafficking of VLDL beyond delivery of FFA. Based on the size similarity of pre-chylomicron transport vesicles (PCTVs) and PG-VTVs, this may be related to post-Golgi trafficking of VLDL, but further study is required to substantiate this hypothesis

It has been observed that cathepsin B is able to translocate to the cytosol upon stimulation with oleic acid or TNFα (12, 13). Analysis of the VTV proteome revealed that LFABP, one of the most abundant cytosolic proteins in hepatocytes, contains the cognate VKM cleavage sequence, which is cleaved by cathepsin B *in vitro* (14). The results of the present study show that knockdown of cathepsin B with siRNA leads to reduced degradation of LFABP, resulting in a 74% increase in LFABP protein expression when exposed to at least 0.4 mM OA complexed with BSA for 1 h. 1 h of OA-BSA exposure was also sufficient to redistribute the staining pattern of cathepsin B and LFABP, inducing co-localization of cathepsin B with LFABP in the cytosol, which was not observed without oleic acid treatment in the present study. A distinct Golgi-like pattern of cathepsin B staining was observable across all dual-labeling experiments and consistent with robust secretion of this protein by the liver. Co-localization of GOS28 with LFABP was observed to a greater extent than with cathepsin B, but OA-BSA did not significantly increase co-localization with either protein as determined by the Pearson coefficient. 24 h after OA-BSA treatment, a slight and not statistically significant increase in the degree of co-localization between LFABP and cathepsin B was observed. However, under these conditions, the degree of cytosolic cathepsin B distribution is increased, as is the nuclear localization of LFABP.

Regulation of LFABP levels by protease cleavage has been suggested previously (34, 35), with reports showing increased stability of LFABP bound to oleic acid. Taken with the present data, this suggests that cathepsin B mediates turnover of LFABP after delivery of FFA cargo. Using overexpression of the VKM → VNL cleavage-resistant LFABP mutant, we established that cathepsin B specifically recognizes and cleaves after the Val-Lys-Met sequence in McA-RH7777 cytosol. This observation was validated physiologically and biochemically, as overexpression of the mutant LFABP resulted in a 20% increase in [^{3}H]TAG associated with VLDL secreted into the medium when compared with cells overexpressing wildtype LFABP after 24 h and a significant 66% increase in LFABP protein, which was also contingent on OA-BSA treatment.

Elevation of cytosolic cathepsin B could be driven by conditions of elevated serum FFA or chronic TNFα production, which are both observed in insulin resistance, and may contribute the progress of hepatic steatosis through the novel mechanism described in this study (36). Thus, the suppression of elevated FFA concentration, or inhibition of cytosolic cathepsin B activity or redistribution, could serve to slow down the progression of hepatic steatosis through restoring functional VLDL secretion and FFA uptake by the liver. A 39% increase in [^{3}H]TAG secretion after 1 h by McA-RH7777 cells supplemented with 0.4 mM OA complexed with BSA for 24 h was observed as a result of cathepsin B knockdown. This is logically supported by a previous twin study (37) showing increased atherosclerotic cardiovascular disease in association with increased cystatin C levels, which is an endogenously produced inhibitor of cathepsin B. This suggests that cathepsin B inhibition may be effective in restoring VLDL secretion and slowing the progress of hepatic steatosis, but this may result in unwanted increases in VLDL secretion and risk for atherosclerotic cardiovascular disease, which must also be managed carefully. Previous studies in NAFLD patients have observed impaired autophagy and suppressed cathepsin B expression (38). This may be a result of prolonged increases in lysosomal permeability, leading to cathepsin B redistribution from the lysosome due to chronically elevated OA-BSA or TNFα exposure. In the aforementioned study, NAFLD patients presented with drastic increases in serum TAG. This is in agreement with our observations in the present study, where cathepsin B knockdown leads to increased VLDL secretion. Increased VLDL secretion observed in the present study was accompanied by a 70% increase in expression of CD36 and LFABP, suggesting increased FFA uptake and distribution for TAG synthesis as a result of cathepsin B knockdown. Without OA pretreatment, [^{3}H]TAG secretion was increased by 15% after 1 h, and CD36 expression increased by 31.5% as a result of cathepsin B knockdown. These results suggest that cathepsin B regulates cellular CD36 and LFABP protein levels and that this mechanism restricts the flow of FFA via LFABP and CD36 for TAG synthesis and VLDL secretion.

This mechanism may help to explain why cathepsin B knockout mice are resistant to diet-induced hepatic steatosis, as cathepsin B knockdown resulted in a 32% decrease in cellular TAG as measured by retention of the [^{3}H]TAG. This observation was attributed to the increase in VLDL-apoB secretion. Interestingly, cathepsin B overexpression resulted in a 24% decrease in [^{3}H]TAG secretion after 2 h as well as a 23% decrease in retention of our [^{3}H]TAG after 24 h of secretion. This is in agreement with decreased FFA uptake during the initial pulse period, which was attributed to decreased expression of LFABP and CD36 under conditions of cathepsin B overexpression.

A role for cathepsin B in regulating gene expression may exist through LFABP cleavage, as LFABP has been shown to deliver

hydrophobic ligands to the nucleus and regulate PPARα signaling (7). Thus, cathepsin B localization may influence PPARα signaling secondary to ligand delivery by LFABP, in addition to the impact on VLDL and FFA trafficking described in the present study. This phenomenon could contribute to worsening dyslipidemia. It has also been observed that PPARα signaling in conjunction with IL-6–mediated inflammation contributes to increased LFABP expression and post-prandial increases in FFA uptake (39). Disruption of this process by cathepsin B could lead to systemic increases in FFA as a result of reduced hepatic FFA uptake by LFABP and CD36, which would most certainly be compensated for by the body in some way, or manifest in a pathology. Elevated serum FFA would lead to inflammation and peripheral insulin resistance as a result of the toxic effect of elevated serum FFA. This could have a downstream impact of increased pyruvate carboxylase flux and thus lead to the progression of type II diabetes mellitus by elevating hepatic acetyl-CoA (40).

Experimental procedures

Reagents

Immunoblot reagents were attained from Bio-Rad. ECL (enhanced chemiluminescence) reagents were purchased from GE Healthcare. Albumin was purchased from Sigma. Recombinant rat growth hormone was purchased from Abcam (catalog no. ab68388). Other reagents were of analytical grade and purchased from local vendors. Ames dwarf (df/df) mice were a gift of Dr. Michal Masternak. All animal procedures were performed in accordance with University of Central Florida institutional animal care and use committee (IACUC) guidelines and in strict agreement with the IACUC-approved protocol.

Antibodies and recombinant proteins

Rabbit polyclonal antibodies targeting cathepsin B, apoB, and LFABP were purchased from Santa Cruz Biotechnology. Anti-rabbit IgG antibodies conjugated to HRP were purchased from Santa Cruz Biotechnology. Wildtype recombinant rat LFABP was purchased from Novus Biologicals (Littleton, CO). Mutant rat LFABP (VKM → VNL; amino acids 83–85) was generated commercially (GenScript USA Inc., Piscataway, NJ). Recombinant rat cathepsin B protein was purchased from Lifespan BioSciences, Inc. (Seattle, WA).

Cell culture

Rat hepatoma cells (McA-RH7777 cells) obtained from American Type Culture Collection (ATCC) were maintained on Dulbecco's modified Eagle's medium (Life Technologies) supplemented with 5% fetal bovine serum (ATCC) and 1% penicillin/streptomycin (Sigma). Additional treatments were performed as indicated in the figure legends. Cell lysates were collected with radioimmune precipitation assay buffer (Thermo Scientific, Rockford, IL). Lysis and extraction buffer was supplemented with protease inhibitor (Roche Applied Science) according to the manufacturer's instructions.

Immunoblotting

Protein concentrations were determined by the Bradford method as described previously (8). Samples were resolved by SDS-PAGE with gel concentrations indicated in figure legends. Proteins were then transferred to nitrocellulose membranes (Bio-Rad), and detection was performed using ECL (GE Healthcare) and autoradiography film (MIDSCI, St. Louis, MO).

2D-DIGE

Samples were prepared resolved, and analyzed according to the manufacturer's instructions. Briefly, an equal mass of protein was labeled with Cy3 or Cy5 fluorescent dye. The samples were then mixed, loaded onto an 11-cm IPG strip, and subjected to isoelectric focusing for 21 h using a total of 50,500 V-h. After isoelectric focusing, the IPG strip was equilibrated, loaded onto a 4–20% gradient Tris-HCl gel, resolved, and scanned using a Typhoon TRIO imager (GE Healthcare). The ExPASy protein database was used for putative identification of protein spots.

Treatment of hepatocytes with oleic acid

Rat hepatocytes (McA-RH7777 cells) were washed with warm (37 °C) PBS and incubated with 0.4 mM OA complexed with BSA in DMEM containing 5% FBS for either 1 or 24 h (as indicated in the figure legends). For the control, cells were treated with BSA (0.2 mM) alone in DMEM.

Pulse labeling

[^{3}H]Oleic acid (45.5 Ci/mm) was purchased from PerkinElmer Life Sciences. For pulse-labeling experiments, 0.3×10^6 cells were plated in each well of a 6-well plate. Transfections were performed simultaneously with plating as described below. For experiments requiring RNA interference, medium was discarded after 48 h, and the cells were washed twice using fresh medium without penicillin/streptomycin. Cells were incubated in 0.4 mM OA complexed with BSA containing 2 μCi of BSA-bound [^{3}H]oleic acid for 1 h. The pulse was then discarded, and the cells were washed twice as described previously to remove residual labeled oleic acid and given fresh 5% FBS-containing DMEM. 200-μl aliquots were taken at the indicated time intervals. Radioactivity (dpm) associated with [^{3}H]TAG was measured from 100-μl medium aliquots by liquid scintillation counting using a Tri-Carb 2910TR liquid scintillation analyzer (PerkinElmer Life Sciences). For experiments requiring plasmid transfection, cells were removed from transfection medium after 4 h of exposure, given fresh medium, and pulsed 48 h after plating as described.

TAG extraction

Protein concentrations were determined by the Bradford method as described previously (8). Whole-cell lysates from McA-RH7777 cells were collected as described previously, with any prior treatment indicated in the figure legend. 50 μg of whole cell lysate protein with [^{3}H]TAG was diluted to 200 μl with PBS and mixed with 1.5 ml of isopropyl alcohol/*n*-heptane/deionized H_2O (80/20/2; v/v/v), vortexed vigorously, and allowed to settle. 1 ml of *n*-heptane and 0.5 ml of deionized H_2O were added. The mixture was vortexed thoroughly and then spun until separation of the organic layer. The organic layer was collected and mixed with 2 ml of 0.5 N NaOH/EtOH/deionized H_2O (1/5/5; v/v/v), vortexed vigorously, and spun until separa-

tion of the organic layer. The organic layer (*n*-heptane) containing [^{3}H]TAG was subjected to liquid scintillation counting as described previously (28, 41–43).

siRNA transfection

McA-RH7777 cells were transfected using Lipofectamine RNAiMax (ThermoFisher Scientific) according to the manufacturer's instructions. A final concentration of 25 nM cathepsin B siRNA (Silencer select predesigned siRNA, Life Technologies, catalog no. s134210) was used as indicated. To exclude or minimize off-target effects of siRNA, we utilized several approaches. First, we used different concentrations of siRNA for optimization and used the minimal concentration that gave the maximal knockdown. Second, we used several siRNA against the same target and used different transfection protocols.

Preparation of ER, Golgi, lysosomes, and cytosol

For the preparation of ER and Golgi, McA-RH7777 cells were washed once with buffer A (136 mM NaCl, 11.6 mM KH_2PO_4, 8 mM Na_2HPO_4, 7.5 mM KCl, 0.5 mM dithiothreitol, pH 7.2) and resuspended in 0.25 M sucrose in 10 mM Hepes containing 50 mM EDTA and protease inhibitors (Roche Diagnostics GmbH, Mannheim, Germany) and homogenized using Parr cell disruption vessel at 1,100 p.s.i. for 40 min followed by isolation and purification of the ER and Golgi using a sucrose step gradient as described previously (25, 44).

Lysosomes were prepared using a slight modification of the method described by Stahn *et al.* (45). In brief, McA-RH7777 cells were washed once with buffer A and resuspended in 0.25 M sucrose in 10 mM Hepes containing 50 mM EDTA and protease inhibitors (Roche Diagnostics GmbH) and homogenized using a Parr cell disruption vessel at 1,100 p.s.i. for 40 min followed by spinning of the homogenate at 750 × *g* for 10 min. The pellet was discarded, and the post-nuclear supernatant was centrifuged at 3,300 × *g* for 10 min. The supernatant (post-mitochondrial) was collected and spun at 16,000 × *g* for 20 min, and the pellet containing lysosomes was collected.

Cytosol was prepared from McA-RH7777 cells using the same procedure as reported earlier (25, 44)). In brief, McA-RH7777 cells were washed once with buffer B (25 mM Hepes, 125 mM KCl, 2.5 mM $MgCl_2$, 0.5 mM DTT, and protease inhibitors, pH 7.2) and homogenized using a Parr cell disruption vessel at 1,100 p.s.i. for 40 min, followed by ultracentrifugation at 40,000 rpm for 95 min (Beckman Rotor 70.1 Ti). The resultant supernatant (cytosol) was collected, dialyzed overnight against cold buffer B at 4 °C, and then concentrated to a final concentration of protein ~20 mg/ml using a Centricon filter (Amicon, Beverly, MA) with a 10-kDa cutoff.

Plasmid transfection

pCI-Neo vector containing rat Cathepsin B gene insert (RefSeq number NM_022597.2) and pCI-Neo vector containing rat wildtype LFABP gene insert (RefSeq number NM_012556.2) or cathepsin B-resistant mutant LFABP gene insert were purchased from Life Technologies. Transfection was carried out using Lipofectamine 2000 according to the manufacturer's instructions.

Statistical analysis

Data were compared using GraphPad software (GraphPad Prism version 5 software for Mac OS X version) employing either a two-tailed *t* test or a one-way analysis of variance (ANOVA).

Author contributions—S. T. designed and carried out the experiments and analyzed the results. S. S. performed all small animal surgeries to isolate primary hepatocytes, carried out confocal and immunoblotting experiments, and analyzed the results. S. S. and F. M. performed 2D-DIGE experiments. O. Z. performed several experiments to ascertain the reproducibility. M. M. M. provided Ames dwarf mice and analyzed the results. S. A. S. conceived and designed the experiments and analyzed the results. S. T. and S. A. S. wrote the paper.

References

1. Ota, T., Gayet, C., and Ginsberg, H. N. (2008) Inhibition of apolipoprotein B100 secretion by lipid-induced hepatic endoplasmic reticulum stress in rodents. *J. Clin. Invest.* **118,** 316–332 CrossRef Medline
2. Fisher, E. A. (2012) The degradation of apolipoprotein B100: multiple opportunities to regulate VLDL triglyceride production by different proteolytic pathways. *Biochim. Biophys. Acta* **1821,** 778–781 CrossRef Medline
3. Howell, K. W., Meng, X., Fullerton, D. A., Jin, C., Reece, T. B., and Cleveland, J. C., Jr. (2011) Toll-like receptor 4 mediates oxidized LDL-induced macrophage differentiation to foam cells. *J. Surg. Res.* **171,** e27–e31 CrossRef Medline
4. Ginsberg, H. N. (2002) New perspectives on atherogenesis role of abnormal triglyceride-rich lipoprotein metabolism. *Circulation* **106,** 2137–2142 CrossRef Medline
5. Tiwari, S., and Siddiqi, S. A. (2012) Intracellular trafficking and secretion of VLDL. *Arterioscler. Thromb. Vasc. Biol.* **32,** 1079–1086 CrossRef Medline
6. Coburn, C. T., Hajri, T., Ibrahimi, A., and Abumrad, N. A. (2001) Role of CD36 in membrane transport and utilization of long-chain fatty acids by different tissues. *J. Mol. Neurosci.* **16,** 117–121; discussion 151–117 CrossRef Medline
7. Storch, J., and McDermott, L. (2009) Structural and functional analysis of fatty acid-binding proteins. *J. Lipid Res.* **50,** S126–S131 CrossRef Medline
8. Shelness, G. S., Ingram, M. F., Huang, X. F., and DeLozier, J. A. (1999) Apolipoprotein B in the rough endoplasmic reticulum: translation, translocation and the initiation of lipoprotein assembly. *J. Nutr.* **129,** 456S–462S Medline
9. Keller, U., and Miles, J. M. (1991) Growth hormone and lipids. *Horm. Res.* **36,** 36–40 CrossRef Medline
10. Elam, M. B., Wilcox, H. G., Solomon, S. S., and Heimberg, M. (1992) *In vivo* growth hormone treatment stimulates secretion of very low density lipoprotein by the isolated perfused rat liver. *Endocrinology* **131,** 2717–2722 CrossRef Medline
11. Frick, F., Lindén, D., Améen, C., Edén, S., Mode, A., and Oscarsson, J. (2002) Interaction between growth hormone and insulin in the regulation of lipoprotein metabolism in the rat. *Am. J. Physiol. Endocrinol. Metab.* **283,** E1023–E1031 CrossRef Medline
12. Feldstein, A. E., Werneburg, N. W., Canbay, A., Guicciardi, M. E., Bronk, S. F., Rydzewski, R., Burgart, L. J., and Gores, G. J. (2004) Free fatty acids promote hepatic lipotoxicity by stimulating TNF-α expression via a lysosomal pathway. *Hepatology* **40,** 185–194 CrossRef Medline
13. Feldstein, A. E., Werneburg, N. W., Li, Z., Bronk, S. F., and Gores, G. J. (2006) Bax inhibition protects against free fatty acid-induced lysosomal permeabilization. *Am. J. Physiol. Gastrointest. Liver Physiol.* **290,** G1339–G1346 CrossRef Medline
14. Hook, V., Funkelstein, L., Wegrzyn, J., Bark, S., Kindy, M., and Hook, G. (2012) Cysteine cathepsins in the secretory vesicle produce active pep-

tides: cathepsin L generates peptide neurotransmitters and cathepsin B produces β-amyloid of Alzheimer's disease. *Biochim. Biophys. Acta* **1824,** 89–104 CrossRef Medline
15. Rahim, A., Nafi-valencia, E., Siddiqi, S., Basha, R., Runyon, C. C., and Siddiqi, S. A. (2012) Proteomic analysis of the very low density lipoprotein (VLDL) transport vesicles. *J. Proteomics* **75,** 2225–2235 CrossRef Medline
16. Brown-Borg, H. M., Borg, K. E., Meliska, C. J., and Bartke, A. (1996) Dwarf mice and the ageing process. *Nature* **384,** 33 CrossRef Medline
17. Masternak, M. M., and Bartke, A. (2012) Growth hormone, inflammation and aging. *Pathobiol. Aging Age Relat. Dis.* **2,** CrossRef Medline
18. Wang, Z., Al-Regaiey, K. A., Masternak, M. M., and Bartke, A. (2006) Adipocytokines and lipid levels in Ames dwarf and calorie-restricted mice. *J. Gerontol. A Biol. Sci. Med. Sci.* **61,** 323–331 CrossRef Medline
19. Guicciardi, M. E., Miyoshi, H., Bronk, S. F., and Gores, G. J. (2001) Cathepsin B knockout mice are resistant to tumor necrosis factor-α-mediated hepatocyte apoptosis and liver injury: implications for therapeutic applications. *Am. J. Pathol.* **159,** 2045–2054 CrossRef Medline
20. Storch, J., and Corsico, B. (2008) The emerging functions and mechanisms of mammalian fatty acid-binding proteins. *Annu. Rev. Nutr.* **28,** 73–95 CrossRef Medline
21. Elovson, J., Chatterton, J. E., Bell, G. T., Schumaker, V. N., Reuben, M. A., Puppione, D. L., Reeve, J. R., Jr., and Young, N. L. (1988) Plasma very low density lipoproteins contain a single molecule of apolipoprotein B. *J. Lipid Res.* **29,** 1461–1473 Medline
22. Fisher, E. A., Khanna, N. A., and McLeod, R. S. (2011) Ubiquitination regulates the assembly of VLDL in HepG2 cells and is the committing step of the apoB-100 ERAD pathway. *J. Lipid Res.* **52,** 1170–1180 CrossRef Medline
23. Sparks, J. D., Sparks, C. E., and Adeli, K. (2012) Selective hepatic insulin resistance, VLDL overproduction, and hypertriglyceridemia. *Arterioscler. Thromb. Vasc. Biol.* **32,** 2104–2112 CrossRef Medline
24. Ginsberg, H. N., and Fisher, E. A. (2009) The ever-expanding role of degradation in the regulation of apolipoprotein B metabolism. *J. Lipid Res.* **50,** S162–S166 CrossRef Medline
25. Siddiqi, S. A. (2008) VLDL exits from the endoplasmic reticulum in a specialized vesicle, the VLDL transport vesicle, in rat primary hepatocytes. *Biochem. J.* **413,** 333–342 CrossRef Medline
26. Siddiqi, S., Mani, A. M., and Siddiqi, S. A. (2010) The identification of the SNARE complex required for the fusion of VLDL-transport vesicle with hepatic cis-Golgi. *Biochem. J.* **429,** 391–401 CrossRef Medline
27. Tiwari, S., Siddiqi, S., and Siddiqi, S. A. (2013) CideB protein is required for the biogenesis of very low density lipoprotein (VLDL) transport vesicle. *J. Biol. Chem.* **288,** 5157–5165 CrossRef Medline
28. Tiwari, S., Siddiqi, S., Zhelyabovska, O., and Siddiqi, S. A. (2016) Silencing of small valosin-containing protein-interacting protein (SVIP) reduces very low density lipoprotein (VLDL) secretion from rat hepatocytes by disrupting its endoplasmic reticulum (ER)-to-Golgi trafficking. *J. Biol. Chem.* **291,** 12514–12526 CrossRef Medline
29. Tran, K., Thorne-Tjomsland, G., DeLong, C. J., Cui, Z., Shan, J., Burton, L., Jamieson, J. C., and Yao, Z. (2002) Intracellular assembly of very low density lipoproteins containing apolipoprotein B100 in rat hepatoma McA-RH7777 cells. *J. Biol. Chem.* **277,** 31187–31200 CrossRef Medline
30. Swift, L. L. (1996) Role of the Golgi apparatus in the phosphorylation of apolipoprotein B. *J. Biol. Chem.* **271,** 31491–31495 Medline
31. Yamaguchi, J., Gamble, M. V., Conlon, D., Liang, J. S., and Ginsberg, H. N. (2003) The conversion of apoB100 low density lipoprotein/high density lipoprotein particles to apoB100 very low density lipoproteins in response to oleic acid occurs in the endoplasmic reticulum and not in the Golgi in McA RH7777 cells. *J. Biol. Chem.* **278,** 42643–42651 CrossRef Medline
32. Higgins, J. A. (1988) Evidence that during very low-density lipoprotein assembly in rat hepatocytes most of the triacylglycerol and phospholipid are packaged with apolipoprotein B in the Golgi complex. *FEBS Lett.* **232,** 405–408 CrossRef Medline
33. Hossain, T., Riad, A., Siddiqi, S., Parthasarathy, S., and Siddiqi, S. A. (2014) Mature VLDL triggers the biogenesis of a distinct vesicle from the trans-Golgi network for its export to the plasma membrane. *Biochem. J.* **459,** 47–58 CrossRef Medline
34. Honma, Y., Niimi, M., Uchiumi, T., Takahashi, Y., and Odani, S. (1994) Evidence for conformational change of fatty acid-binding protein accompanying binding of hydrophobic ligands. *J. Biochem.* **116,** 1025–1029 CrossRef Medline
35. Carlsson, L., Lindén, D., Jalouli, M., and Oscarsson, J. (2001) Effects of fatty acids and growth hormone on liver fatty acid binding protein and PPARalpha in rat liver. *Am. J. Physiol. Endocrinol. Metab.* **281,** E772–E781 CrossRef Medline
36. Reaven, G. M., and Chen, Y. D. I. (1988) Role of abnormal free fatty acid metabolism in the development of non-insulin-dependent diabetes mellitus. *Am. J. Med.* **85,** 106–112 CrossRef Medline
37. Arpegård, J., Magnusson, P. K., Chen, X., Ridefelt, P., Pedersen, N. L., De Faire, U., and Svensson, P. (2016) Cystatin C predicts incident cardiovascular disease in twins. *J. Am. Heart Assoc.* **5,** e003085 CrossRef Medline
38. Fukuo, Y., Yamashina, S., Sonoue, H., Arakawa, A., Nakadera, E., Aoyama, T., Uchiyama, A., Kon, K., Ikejima, K., and Watanabe, S. (2014) Abnormality of autophagic function and cathepsin expression in the liver from patients with non-alcoholic fatty liver disease. *Hepatol. Res.* **44,** 1026–1036 CrossRef Medline
39. Vida, M., Serrano, A., Romero-Cuevas, M., Pavón, F. J., González-Rodriguez, A., Gavito, A. L., Cuesta, A. L., Valverde, A. M., Rodríguez de Fonseca, F., and Baixeras, E. (2013) IL-6 cooperates with peroxisome proliferator-activated receptor-α-ligands to induce liver fatty acid binding protein (LFABP) up-regulation. *Liver Int.* **33,** 1019–1028 CrossRef Medline
40. Perry, R. J., Camporez, J. P., Kursawe, R., Titchenell, P. M., Zhang, D., Perry, C. J., Jurczak, M. J., Abudukadier, A., Han, M. S., Zhang, X. M., Ruan, H. B., Yang, X., Caprio, S., Kaech, S. M., Sul, H. S., *et al.* (2015) Hepatic acetyl CoA links adipose tissue inflammation to hepatic insulin resistance and type 2 diabetes. *Cell* **160,** 745–758 CrossRef Medline
41. Kumar, N. S., and Mansbach, C. M. (1997) Determinants of triacylglycerol transport from the endoplasmic reticulum to the Golgi in intestine. *Am. J. Physiol.* **273,** G18–G30 Medline
42. Siddiqi, S. A., Gorelick, F. S., Mahan, J. T., and Mansbach, C. M., 2nd (2003) COPII proteins are required for Golgi fusion but not for endoplasmic reticulum budding of the pre-chylomicron transport vesicle. *J. Cell Sci.* **116,** 415–427 CrossRef Medline
43. Neeli, I., Siddiqi, S. A., Siddiqi, S., Mahan, J., Lagakos, W. S., Binas, B., Gheyi, T., Storch, J., and Mansbach, C. M., 2nd. (2007) Liver fatty acid-binding protein initiates budding of pre-chylomicron transport vesicles from intestinal endoplasmic reticulum. *J. Biol. Chem.* **282,** 17974–17984 CrossRef Medline
44. Siddiqi, S. A. (2015) *In vitro* analysis of the very-low density lipoprotein export from the trans-Golgi network. *Curr. Protoc. Cell Biol.* **67,** 11.21.1–11.21.17 CrossRef Medline
45. Stahn, R., Maier, K.-P., and Hannig, K. (1970) A new method for the preparation of rat liver lysosomes. *J. Cell Biol.* **46,** 576–591 CrossRef Medline